

### 3. THE EFFECT OF CRACKS ON THE SEISMIC VELOCITIES OF BASALT FROM SITE 990, SOUTHEAST GREENLAND MARGIN<sup>1</sup>

Brian Cerney<sup>2,3</sup> and Richard L. Carlson<sup>2</sup>

#### ABSTRACT

Seismic velocities in rocks are influenced by the properties of the solid, the pore fluid, and the pore space. Cracks dramatically affect seismic velocities in rocks; their influence on the effective elastic moduli of rocks depends on their shape and concentration. Thin cracks (or fractures) substantially lower the moduli of a rock relative to the effect of spherical voids (or vesicles), and lower moduli are reflected by lower *P*- and *S*-wave velocities. The objective of this research is to determine the types and concentrations of cracks and their influence on the seismic properties of subaerially erupted basalts drilled from Hole 990A on the Southeast Greenland margin during Ocean Drilling Program Leg 163. Ellipsoidal cracks are used to model the voids in the rocks. The elastic moduli of the solid (grains) are also free parameters in the inverse modeling procedure. The apparent grain moduli reflect a weighted average of the moduli of the constituent minerals (e.g., plagioclase, augite, and clay minerals). The results indicate that (1) there is a strong relationship between *P*-wave velocity and porosity, suggesting a similarity of pore shape distributions, (2) the distribution of crack types within the massive, central region of aa flows from Hole 990A is independent of total porosity, (3) thin cracks are the first to be effectively sealed by alteration products, and (4) grain densities (an alteration index) and apparent grain moduli of the basalt samples are directly related.

#### INTRODUCTION

Ocean Drilling Program (ODP) Hole 990A was drilled along the Southeast Greenland margin during Leg 163 in a water depth of 542 m. The hole was drilled to a total depth of 343 meters below seafloor (mbsf), including 212 m of sediment overlying 131 m of igneous basement comprising 13 basaltic lava flow units (Duncan et al., 1996). Core recovery within the basement was ~80%. The lava flows, which were subaerially erupted from a volcanic rift similar to the modern-day Iceland rift zone, have been dated to ~56 Ma (Tegner and Duncan, Chap. 6, this volume), the approximate time of the initial opening of the North Atlantic Ocean. (It is presumed that a hot spot existed at this site and time and caused extensive volcanism.)

Downhole sonic logs from similar geologic sections (e.g., Hole 642E on the Outer Vøring Plateau and Hole 917A on the Southeast Greenland margin) have shown the *P*-wave velocity to vary within subaerially erupted, basalt flow units (e.g., Shipboard Scientific Party, 1987; Barton et al., 1989; Shipboard Scientific Party, 1994; Planke, 1994). The *P*-wave velocity is lowest at the flow top and bottom (typically 2–5 km s<sup>-1</sup>) and is higher in the massive, central region of the flow unit (typically 5–6.5 km s<sup>-1</sup>) (e.g., Planke, 1994; Duncan et al., 1996; Planke and Cambray, 1998; Planke et al., Chap. 2, this volume). The variation of *P*-wave velocity is caused by variations in the moduli of the solid and variations in porosity and pore shape distributions (assuming that the pore fluid is constant). Generally, there is a greater percentage of low-modulus alteration products (e.g., clays) and pore space in the flow tops and bottoms than in the massive central regions (Shipboard Scientific Party, 1996; Planke and Cambray, 1998). This difference may cause the observed variation of seismic velocities.

Voids, in the form of vesicles and cracks that occur in subaerially erupted basalts, are the result of degassing of the lava and of fracturing and alteration. The amounts and types of voids affect the seismic

velocities of rocks (e.g., Cheng and Toksöz, 1979; Berryman, 1980; Wilkens et al., 1991; Berge et al., 1992). Seismic velocities in basalt can be readily measured both in situ and in the laboratory. Thus, by using appropriate crack theories, we should be able to model void types and distributions within igneous flow units from high-resolution in situ and laboratory seismic data. The primary purpose of this research is to use the theory of Kuster and Toksöz (1974) to assess the effects of crack variations and apparent grain moduli on the seismic velocities of subaerially erupted basalt recovered from Hole 990A. The principal results are that (1) there is a strong relationship between *P*-wave velocity and porosity for this suite of samples, suggesting a similarity of pore shape distributions among the samples, (2) a simple, average, normalized aspect ratio distribution explains the velocity data from the massive central region of the basaltic flow units to within a root-mean-square (RMS) misfit of 0.050 km s<sup>-1</sup>, (3) a greater percentage of higher aspect ratio (more equant) voids is present in the more altered samples, and (4) grain densities (an alteration index) and apparent grain moduli of the basaltic samples are directly related.

#### CRACK MODELS

The effect of voids on the seismic velocities of rocks and composites has been studied by many researchers (e.g., Eshelby, 1957; Mal and Knopoff, 1967; Mori and Tanaka, 1973; Kuster and Toksöz, 1974; Gangi, 1978, 1981; Carlson and Gangi, 1985; Wilkens et al., 1991; Berge et al., 1992; Ju and Chen, 1994; Berryman and Berge, 1996). In general, these studies show that when porosity is held constant, thinner voids (cracks) lower the seismic velocities significantly more than spherical pores, or vesicles (e.g., fig. 1 of Toksöz et al., 1976). This effect is caused by the more substantial lowering of both the bulk and shear moduli of the rock (the effective moduli) when cracks, rather than vesicles, are present. For example, given a hypothetical basalt composed of 50% plagioclase and 50% augite with a porosity of 5%, the effect of spherical voids (e.g., vesicles) is to lower the *P*- and *S*-wave velocities by 4% and 3%, respectively, whereas the effect of voids with an aspect ratio of 0.1 (i.e., the length of the semi-minor axis is one-tenth that of the semi-major axis) is to lower the *P*- and *S*-wave velocities by 13% and 15%, respectively (e.g., Toksöz et al., 1976). Hence, the shapes of the voids and cracks that

<sup>1</sup>Larsen, H.C., Duncan, R.A., Allan, J.F., Brooks, K. (Eds.), 1999. *Proc. ODP, Sci. Results*, 163: College Station, TX (Ocean Drilling Program).

<sup>2</sup>Department of Geology and Geophysics, Texas A&M University, College Station, TX 77843-3115, U.S.A.

<sup>3</sup>Present address: Texaco Upstream Technology, 4800 Fournace Place, Bellaire, TX, 77401-2324, U.S.A. cerneb@texaco.com

populate rocks have a substantial influence on their seismic velocities.

Kuster and Toksöz (1974) proposed a theoretical model in which cracks and voids are approximated by spheroids having different aspect ratios, and the pressure dependence of  $P$ - and  $S$ -wave velocities is accounted for by a distribution or spectrum of spheroids with different aspect ratios. Cheng and Toksöz (1979) developed an inverse procedure for estimating the aspect ratio spectrum of a rock from its measured velocities. The effective elastic moduli of a medium populated by cracks that have  $m$  discrete aspect ratios are given by

$$\frac{K_n^* - K}{K - K} \frac{3K + 4\mu}{3K_n^* + 4\mu} = \sum_{m=1}^M \alpha_m \left[ 1 + \frac{dc}{c}(\alpha_m, P_n) \right] \frac{1}{3} T_1(\alpha_{mn}) \frac{c(\alpha_m)}{\alpha_m}$$

and

$$\frac{\mu_n^* - \mu}{\mu - \mu} \frac{25\mu(3K + 4\mu)}{6\mu_n^*(K + 2\mu) + \mu(9K + 8\mu)} = \sum_{m=1}^M \alpha_m \left[ 1 + \frac{dc}{c}(\alpha_m, P_n) \right] \left[ T_2(\alpha_{mn}) - \frac{1}{3} T_1(\alpha_{mn}) \right] \frac{c(\alpha_m)}{\alpha_m},$$

where  $K_n^*$  and  $\mu_n^*$  are, respectively, the effective bulk and shear moduli of the material at confining pressure  $P_n$ ,  $K$  and  $\mu$  are the bulk and shear moduli of the grains,  $K'$  and  $\mu'$  are the bulk and shear moduli of the pore fluid,  $\alpha_m$  and  $c(\alpha_m)$  are the  $m$ -th aspect ratio and corresponding concentration,  $dc(\alpha_m, P_n)$  is the change in concentration from the initial concentration (at  $P = 0$ ) of cracks with aspect ratio  $\alpha_m$  at confining pressure  $P_n$ , and  $T_1(\alpha_{mn})$  and  $T_2(\alpha_{mn})$  are expressions calculated from the moduli and porosity of the rock (see Kuster and Toksöz, 1974).

The Kuster-Toksöz model does not account for crack-crack interaction. The approximation is therefore valid only for low concentrations of cracks. To have that condition satisfied, Kuster and Toksöz (1974) imposed a limit on the concentrations such that

$$\frac{c_m}{\alpha_m} < 1 \text{ for any } \frac{c_m}{\alpha_m}.$$

We also imposed this constraint, although Berryman (1980) and Berryman and Berge (1996) demonstrated that this strict constraint is not necessary for small  $\alpha_m$  and low porosity samples (e.g.,  $\alpha_m < 0.01$ , and porosity  $< 20\%$ ). Another limitation of the Kuster-Toksöz model is that the modeling results are nonunique and model dependent. Berge et al. (1992) and Berge (1996) have compared various schemes for estimating elastic properties of multiphase composites and have shown the Kuster-Toksöz model to be useful for materials with porosities  $< 20\%$ .

We used the theory of Kuster and Toksöz (1974) to model void-shape distributions using the seismic velocities in samples from Hole 990A. The data used in this study are bulk densities and porosities, and  $P$ - and  $S$ -wave velocities measured at confining pressures ranging from 10–200 MPa in 10 basalt samples from Hole 990A. Porosities were calculated from the measured bulk and grain densities of the samples. The data were inverted for pore aspect ratio distributions and apparent grain moduli using a slightly modified form of the method of Cheng and Toksöz (1979).

## SAMPLES

Upon recovery, cores from Hole 990A were cut into 1.5-m sections and split longitudinally into archive- and working-half cores.  $P$ -wave velocities were measured at 2–5 cm intervals at bench pressure, and first arrivals were picked by eye as soon as possible after core recovery to ensure seawater saturation (Figure 1).

The  $P$ -wave velocities shown in Figure 1 vary from  $\sim 2.2$ – $6.5$  km  $s^{-1}$ . This relatively large range of  $P$ -wave velocities reflects changes

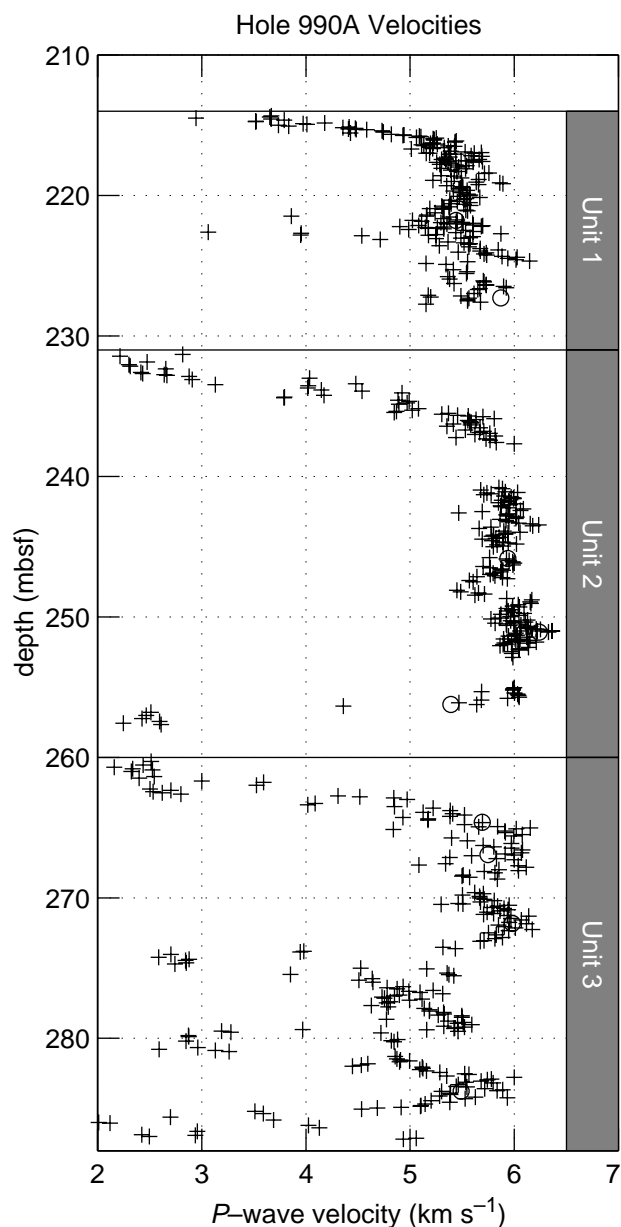


Figure 1. Profile of  $P$ -wave velocity vs. depth measured on board ship at bench pressure on split cores (crosses) and minicores (circles) from the upper three aa flow units from Hole 990A. An absence of data is indicative of little or no core recovery. Measurement precision =  $\pm 0.030$  km  $s^{-1}$ .

in rock properties (e.g., mineralogy and pore shape distribution) down the core. Cyclic velocity patterns are evident throughout the profile. Each full cycle (i.e., low velocity–high velocity–low velocity) corresponds to a single lava flow unit. Shipboard petrologists defined flow boundaries based on visual and microscopic observations of the recovered cores. The petrologically defined flow units correspond to the full cycles observed in the shipboard  $P$ -wave velocity measurements (Fig. 1). The low velocity flow tops and bottoms are characterized by large amounts of alteration products (e.g., clay minerals) and high total porosity. The higher velocity sections consist of massive basalt within the centers of the flow units. Fresh basalt is more prevalent and total porosity is lower in these central sections than in the flow tops and bottoms (Shipboard Scientific Party, 1996; Planke et al., Chap. 2, this volume).

Shipboard petrologists have described the upper three flow units as aa type flows (Shipboard Scientific Party, 1996). We chose to sam-

ple and analyze basalt from the upper three flow units because the distributions of vesicles from these flows are similar. The sample locations and shipboard  $P$ -wave velocity measurements made at bench pressure are shown in Figure 1.

## DATA

The  $P$ - and  $S$ -wave velocities in the seawater-saturated minicores were measured at confining pressures ranging from 10–200 MPa at the Rock Physics Laboratory at Purdue University using the ultrasonic pulse transmission technique of Birch (1960). The samples are 1-in-diameter right cylinders, ~1-in long, drilled perpendicular to the core axis from the split core. The minicores were jacketed with a screen mesh overlain by copper foil. The screen mesh is used to reduce pore pressure buildup, whereas the copper foil prevents the pressure medium from invading the samples at elevated pressures. The grain and bulk densities of the minicores were determined from their masses and volumes, and the porosity for each sample was calculated from the measured densities. Results are reported in Table 1.

Seismic velocity measurements were made at confining pressures ranging to 200 MPa, but samples came from depths between 215 and 275 mbsf, where the in situ differential pressures range from ~4 to 7 MPa. Thus, the velocities measured at the lowest confining pressures (10 MPa) are most nearly representative of the seismic velocities at true in situ pressures and range from 4.7 to 5.9 km s<sup>-1</sup> for the  $P$ -wave data and from 2.8 to 3.4 km s<sup>-1</sup> for the  $S$ -wave data.

The porosities listed in Table 1 range from 2.1% to 6.9%. The bulk porosities correlate very well with the  $P$ -wave velocities made at low pressures (e.g., 10 MPa; Fig. 2A). This strong correlation has been observed in other studies of the physical properties of basalts and diabases (e.g., Wilkens et al., 1983; Christensen and Salisbury, 1985; Barton et al., 1989; Christensen et al., 1989; Carlson and Herrick, 1990; Iturrino, 1995). The correlation shown in Figure 2A suggests that the total porosity has a primary influence on the  $P$ -wave velocities in these samples and that the relative distribution of the pore shapes must be fairly uniform among these samples. A large sample-to-sample variation of the aspect ratio spectra would cause more scatter in the velocity-porosity trend, and the good correlation between  $P$ -wave velocity and porosity would not be observed.

The grain densities listed in Table 1 range from 2740 to 2910 kg m<sup>-3</sup>. The grain densities do not correlate as well with the  $P$ -wave velocities as the bulk porosity, as shown in Figure 2B. The average grain densities on two crushed, almost entirely altered basalt samples is 2100 ± 60 kg m<sup>-3</sup>. Because the density of alteration minerals (largely clays) is lower than the density of the primary minerals in fresh ba-

salts (plagioclase, augite, and olivine), a lower grain density probably indicates a higher percentage of alteration minerals in the samples, so that grain density can be used as a proxy for the relative amount of alteration products.

The  $P$ - and  $S$ -wave data show a smoothly varying velocity-pressure relationship. The scatter in the data from a smooth trend indicates that the measurement error is ± 0.01 km s<sup>-1</sup>. In contrast, the errors in the densities and calculated porosity are not as easy to determine. The estimated uncertainty in the bulk and grain densities is 20 kg m<sup>-3</sup> (<1%); the corresponding error in the porosity is ~1% (one porosity unit).

## MODELING RESULTS

As a rock is compressed, the smallest aspect ratio voids are the first to be effectively closed. Though in reality the crack is never completely closed, it can become sufficiently stiff that the crack moduli approach the grain moduli of the rock. The stiffening of the cracks with increasing confining pressure causes  $P$ - and  $S$ -wave velocities in the rock to increase with confining pressure. This effect has been widely observed (e.g., Adams and Williamson, 1923; Birch, 1960; Christensen, 1982; Iturrino, 1995).

To determine the causes of the velocity variations within the central part of the aa flows and to separate the effect of the pore space from that of the solid rock on the seismic properties of basalt from Hole 990A, we inverted the high-pressure velocity data for the aspect ratio spectrum and apparent grain moduli for each sample listed in Table 1. The linearized form of the Kuster-Toksöz model, as described in Cheng and Toksöz (1979), was used in a constrained, Marquardt least-squares inversion of the velocity data.

The Kuster-Toksöz model does not specify which aspect ratios to use or how to choose which aspect ratios to model. The choice of aspect ratios is arbitrary, and the aspect ratio spectrum obtained by inverting the velocity data is thus nonunique because the aspect ratio spectrum depends on the initial choice of aspect ratios. We modeled the aspect ratio spectra of our samples in two steps. In the first step of the inversion, aspect ratios were chosen so that a specific crack type (as described by its aspect ratio) is effectively closed at each successive pressure increment. For example, the thinnest voids close at 10 MPa, the next set of voids close at 20 MPa, and so on. In addition to the calculated aspect ratios, aspect ratios of 1.0, 0.1, and 0.01 were included in the constrained inversion. A total of 14 different aspect ratios was initially used to model each sample.

The results of the first inversion demonstrated that aspect ratio spectra for the different samples were quite similar, but some calcu-

**Table 1. Bulk and grain density measurements, calculated porosity, and high-pressure  $P$ - and  $S$ -wave velocity measurements for samples from Hole 990A.**

Core, section, interval (cm)	Bulk density (g cm <sup>-3</sup> )	Grain density (g cm <sup>-3</sup> )	Porosity (%)	Mode	Velocity (km s <sup>-1</sup> ) – pressure (MPa)										
					10	20	40	60	80	100	120	140	160	180	200
990A-6R-3, 135–137	2750	2820	6.9	$P$ -wave	4.723	4.827	4.937	5.005	5.055	5.096	5.131	5.161	5.208	5.208	5.208
				$S$ -wave	2.753	2.795	2.839	2.865	2.883	2.898	2.910	2.921	2.930	2.938	2.945
990A-7R-5, 7–9	2860	2900	3.8	$P$ -wave	5.467	5.532	5.605	5.654	5.692	5.723	5.750	5.773	5.793	5.812	5.828
				$S$ -wave	3.092	3.124	3.160	3.183	3.199	3.212	3.222	3.230	3.236	3.242	3.247
990A-10R-1, 12–14	2850	2880	3.0	$P$ -wave	5.622	5.666	5.720	5.756	5.783	5.805	5.822	5.836	5.847	5.857	5.865
				$S$ -wave	3.200	3.226	3.258	3.278	3.292	3.302	3.309	3.315	3.319	3.323	3.326
990A-10R-4, 101–103	2860	2880	2.5	$P$ -wave	5.836	5.941	5.982	6.027	6.064	6.094	6.120	6.143	6.163	6.182	6.198
				$S$ -wave	3.157	3.188	3.226	3.252	3.271	3.285	3.296	3.305	3.312	3.318	3.323
990A-11R-1, 79–81	2870	2890	2.1	$P$ -wave	5.895	5.941	5.992	6.025	6.052	6.074	6.094	6.111	6.127	6.141	6.154
				$S$ -wave	3.382	3.416	3.457	3.481	3.497	3.507	3.514	3.520	3.524	3.527	3.530
990A-12R-1, 125–127	2690	2750	6.1	$P$ -wave	4.907	4.982	5.063	5.116	5.156	5.189	5.217	5.242	5.265	5.285	5.303
				$S$ -wave	2.896	2.926	2.962	2.985	3.000	3.010	3.017	3.023	3.027	3.030	3.032
990A-13R-4, 36–38	2780	2810	3.6	$P$ -wave	5.461	5.536	5.623	5.674	5.702	5.726	5.741	5.752	5.760	5.767	5.773
				$S$ -wave	3.057	3.091	3.125	3.146	3.161	3.173	3.183	3.191	3.198	3.205	3.210
990A-14R-2, 94–96	2690	2740	4.3	$P$ -wave	5.244	5.321	5.417	5.453	5.532	5.572	5.603	5.629	5.650	5.668	5.683
				$S$ -wave	2.990	3.028	3.067	3.091	3.108	3.121	3.132	3.142	3.150	3.158	3.164
990A-15R-2, 101–103	2890	2910	2.6	$P$ -wave	5.915	5.956	6.000	6.027	6.045	6.059	6.070	6.078	6.086	6.092	6.098
				$S$ -wave	3.312	3.333	3.354	3.366	3.374	3.381	3.387	3.391	3.396	3.399	3.403
990A-17R-4, 62–64	2760	2810	4.4	$P$ -wave	5.198	5.267	5.342	5.401	5.432	5.452	5.466	5.476	5.483	5.488	5.493
				$S$ -wave	2.934	2.960	2.984	2.998	3.009	3.017	3.024	3.030	3.036	3.041	3.045

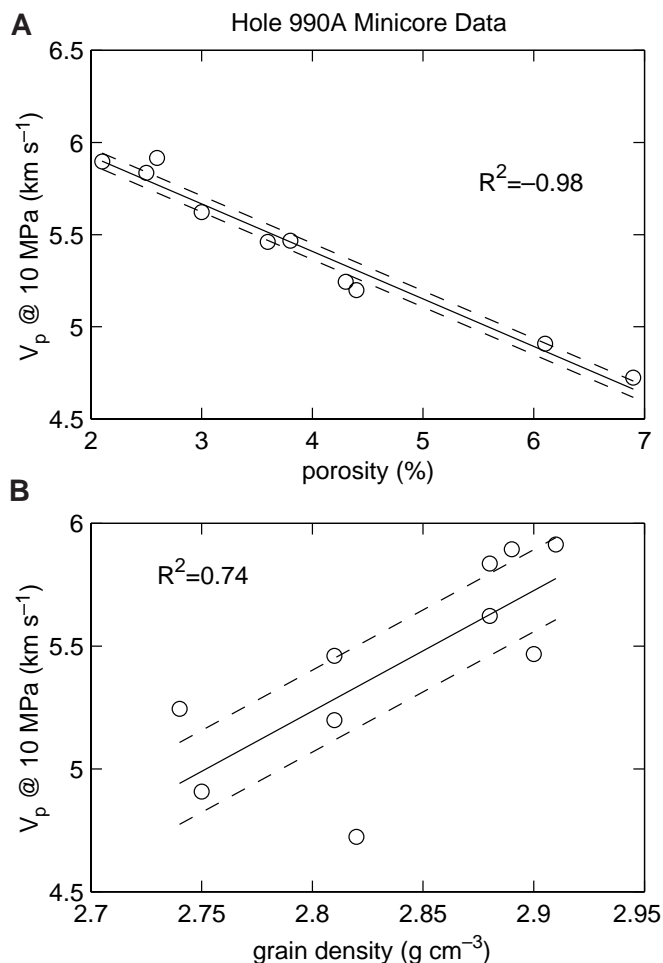


Figure 2.  $P$ -wave velocities ( $V_p$ ) measured at 10 MPa confining pressure vs. (A) porosity and (B) grain density for the basaltic samples used in this study. A least-squares-fit (solid line) is shown along with one standard deviation bounds (dashed line) for (A) and (B). The standard deviations for the fits to (A) and (B) are 0.04 and 0.17  $\text{km s}^{-1}$  respectively. The correlation between  $V_p$  and porosity suggests that the distribution of pore shapes within the samples does not vary much between the samples.

lated aspect ratios were not significantly different and some did not have significant concentrations. In the second step of the inversion, we chose just six aspect ratios that span the range used in the first inversion, 1.0, 0.1, 0.01, 0.005, 0.001, and 0.0005. The criterion for the number of aspect ratios used in the second inversion was that the RMS misfit for each sample modeled be  $<0.050 \text{ km s}^{-1}$  ( $<2\%$  RMS misfit). The results of this second constrained inversion are listed in Table 2, where the void concentrations are reported as porosities (in percent), which means the sum of the concentrations is equal to the porosity of the sample.

To compare the aspect ratio spectra of the samples, we used a normalized aspect ratio spectrum in which the normalized concentration is the total concentration divided by the porosity of the sample. The sum of the normalized aspect ratio concentrations is 1, and the porosity is a scaling factor. The normalized concentrations reveal a similarity in the aspect ratio spectra for the samples shown in Figure 3. Also shown are the averaged normalized concentrations for this suite of samples. The averaged normalized concentration represents the average aspect ratio spectrum for this suite of samples.

The similarity of the aspect ratio spectra for these samples (Fig. 3) suggests that the average of the normalized concentrations might ap-

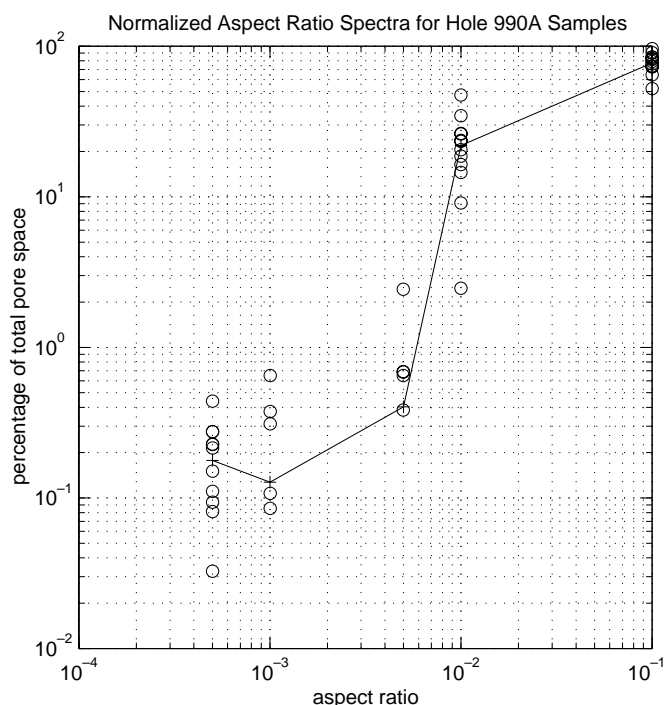


Figure 3. Normalized aspect ratio spectrum for each sample determined by modeling the six aspect ratios listed in Table 2 (circles). The aspect ratio spectrum found for each sample has been normalized by the porosity of the sample. The average normalized aspect ratio spectrum (Table 3) is also shown (crosses).

ply to all of the samples (i.e., that the relative proportions of different cracks in all of the samples are essentially the same). If so, then the  $P$ - and  $S$ -wave velocities in any sample can be estimated from the porosity and the average aspect ratio spectrum with nearly the same accuracy and precision achieved by using the best fitting spectrum for that particular sample (Table 2). To test this hypothesis, we used the average spectrum to calculate the velocities in each sample and compared the calculated velocities with the observed velocities reported in Table 1. An example of the calculated velocities (for Sample 163-990A-10R-1, 12–14 cm) is shown in Figure 4. In all cases, the RMS misfit is  $<0.050 \text{ km s}^{-1}$  ( $<2\%$ ). In two cases, the misfit is increased by a factor of two or three, relative to the misfit for the spectrum of that particular sample. In the remaining eight cases, the misfit is increased by  $<20\%$ . To a very good approximation, these rocks can be described as having the aspect ratio spectrum that is summarized in Table 3.

## ALTERATION EFFECTS

From their analyses of samples from Sites 417 and 418, Christensen et al. (1980) and Carlson and Herrick (1990) showed that the grain densities of oceanic basalts decrease with increasing porosity and suggested that a decrease in grain density reflects an increase in the relative amounts of alteration products. The grain density of the freshest basalt measured in the suite of samples from this study is  $2910 \pm 20 \text{ kg m}^{-3}$ , whereas, the average measured grain density of two almost entirely altered samples is  $2100 \pm 60 \text{ kg m}^{-3}$ . Therefore, we can use grain density as an alteration index, and according to Christensen et al. (1980) and Carlson and Herrick (1990), an increase in relative amounts of alteration products (lower grain densities) should correlate with increasing porosity. The porosities listed in Table 1 correlate inversely with grain densities (or rather, the porosities

**Table 2. Hole 990A modeling results from inverting the high-pressure velocity data for a simplified aspect ratio spectrum.**

Section, interval (cm):	6R-3, 135–137	7R-5, 7–9	10R-1, 12–14	10R-4, 101–103	11R-1, 79–81
Aspect ratio	Concentration (%)				
1.0	0	0	0	0	0
0.1	5.85	2.77	2.21	1.42	1.10
0.01	1.00	1.00	0.784	1.00	0.995
0.005	0.0340	0.0261	0	0.0676	0
0.001	0.0106	0	0	0	0
0.0005	0.00561	0.00862	0.00827	0.00917	0.00924
RMS inversion misfit (km s <sup>-1</sup> )	0.038	0.027	0.017	0.021	0.013
RMS average spectrum misfit (km s <sup>-1</sup> )	0.038	0.031	0.019	0.046	0.036

Section, interval (cm):	12R-1, 125–127	13R-4, 36–38	14R-2, 94–96	15R-2, 101–103	17R-4, 62–64
Aspect ratio	Concentration (%)				
1.0	0	0	0	0	0
0.1	5.07	2.73	3.18	2.05	3.58
0.01	1.00	0.854	1.00	0.548	0.817
0.005	0.0234	0	0.110	0	0
0.001	0	0.00312	0	0	0
0.0005	0.00496	0.00991	0.00588	0.00588	0.00414
RMS inversion misfit (km s <sup>-1</sup> )	0.037	0.028	0.040	0.014	0.033
RMS average spectrum misfit (km s <sup>-1</sup> )	0.039	0.031	0.047	0.016	0.033

Note: The root-mean-square (RMS) model misfits to the high-pressure  $P$ - and  $S$ -wave data calculated from modeling an average aspect ratio spectrum are also tabulated.

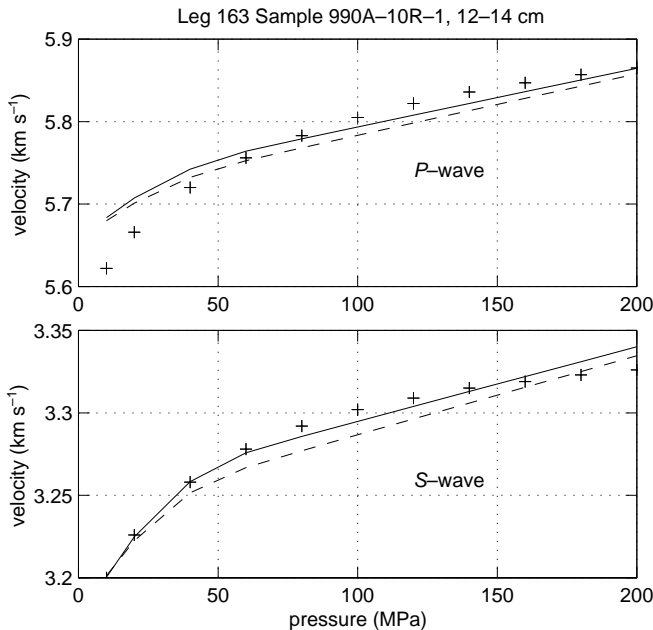


Figure 4.  $P$ - and  $S$ -wave velocity vs. confining pressure measured on Sample 163-990A-10R-1, 12–14 cm (crosses). Also shown are the velocities calculated from the best fitting aspect ratio spectrum determined in the second inversion of the data according to the theory of Kuster-Toksöz (1974) (solid line). The free parameters that were determined in the inversion are the aspect ratio spectrum and the bulk and shear grain moduli. Six different aspect ratios were modeled in this fit to the data. The RMS model misfit for the second inversion is  $0.017 \text{ km s}^{-1}$ . The  $P$ - and  $S$ -wave velocities calculated from the average aspect ratio spectrum from Table 3 are also shown (dashed lines) and have an RMS misfit of only  $0.019 \text{ km s}^{-1}$ . Note the similarity between the two model fits (i.e., between the solid and dashed lines). The aspect ratio spectra and RMS misfits for other samples are listed in Table 2.

**Table 3. Aspect ratio vs. average normalized concentration for the suite of samples modeled.**

Aspect ratio	Concentration (%)
0.1	$77 \pm 3.5$
0.01	$22 \pm 3.5$
0.005	$0.25 \pm 0.15$
0.001	$0.13 \pm 0.05$
0.0005	$0.19 \pm 0.04$

directly correlate with relative amount of alteration) as shown graphically in Figure 5A.

It has also been suggested that the infilling of pore space by alteration products initially closes or heals the thinnest aspect ratio pores, or cracks, because they require the least amount of material to fill (e.g., Wilkens et al., 1991). If this is the case, then there should be a relationship between the amount of pore space represented by thin cracks and the amount of alteration products represented by grain density in the samples. As can be seen in Figure 5B, there is a direct relationship between the percentage of total porosity with aspect ratios  $\leq 0.01$  and grain density, which is an indicator of the amount of alteration. Samples that are more altered have a smaller percentage of the total pore space present as thin aspect ratio voids, even though the bulk porosity is higher in these samples. This is a second-order effect compared to the normalized, average crack spectrum mentioned above, but it does suggest that the thinner cracks are the first to become effectively sealed by alteration products, assuming that the rocks had similar aspect ratio spectra when they were fresh.

Tosaya (1982) measured the  $P$ - and  $S$ -wave velocities and densities of clay-bearing sandstones from the Gulf of Mexico and calculated the bulk and shear moduli from the data. Dvorkin and Nur (1996) later extrapolated the bulk and shear moduli values calculated by Tosaya (1982) to predict the moduli of a zero-porosity rock composed of 100% clays (assumed to be smectites) and reported bulk and shear moduli of 21 and 7 GPa, respectively, for the clay (smectite) minerals. The clay moduli values of Dvorkin and Nur (1982) are lower than the basalt grain bulk and shear moduli values reported by Toksöz et al. (1976), 95 and 42 GPa, respectively. The addition of clay minerals into a basaltic rock will thus lower the grain moduli of

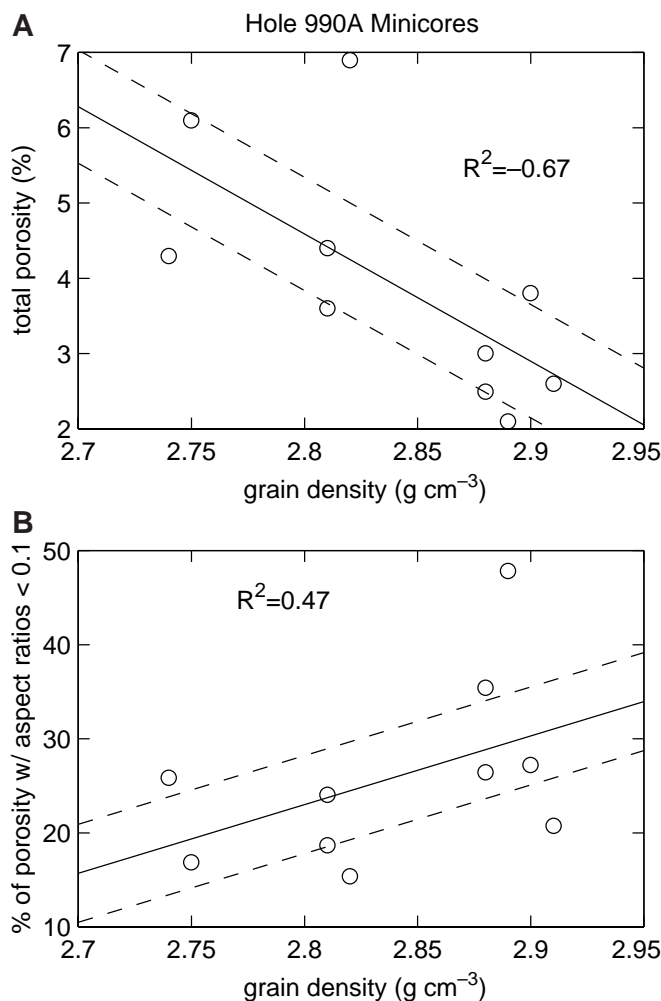


Figure 5. (A) Total porosity and (B) percent of total porosity with aspect ratios < 0.1 vs. grain density. A least-squares-fit (solid line) is shown along with one standard deviation bounds (dashed lines) for (A) and (B). The standard deviations for the fits to (A) and (B) are 0.75% and 5.2%, respectively. Again, grain density is indicative of the relative amount of alteration products, with lower grain densities reflecting a higher percentage of alteration products. These results show a trend toward a lower percentage of thin cracks present in the more altered samples, even though the bulk porosity is higher in these samples. This relationship suggests that the thin cracks are the first pores to be filled by alteration.

the rock in proportion to the relative amount of clays added (Hashin and Shtrikman, 1963).

The apparent grain bulk and shear moduli were used as free parameters in the inversions. Assuming that the Kuster-Toksöz model is a valid construct and assuming that the alteration products consist largely of clays, the apparent grain moduli derived from the models should directly correlate with grain density (or inversely with relative amounts of alteration). The best fitting bulk and shear grain moduli of the samples from Hole 990A are plotted vs. grain density in Figure 6. A direct linear relationship is observed between the apparent bulk and shear grain moduli from the models and the grain densities for this suite of samples, suggesting that the elastic moduli of the solid are significantly affected by alteration. Figure 6 thus shows how an increase in the percentage of low density minerals (presumably alteration products such as clays) lowers the apparent bulk and shear moduli of the grains. Using the least-squares fit to the modeling results (Fig. 6), when the grain density lowers from 2970 to 2740 kg

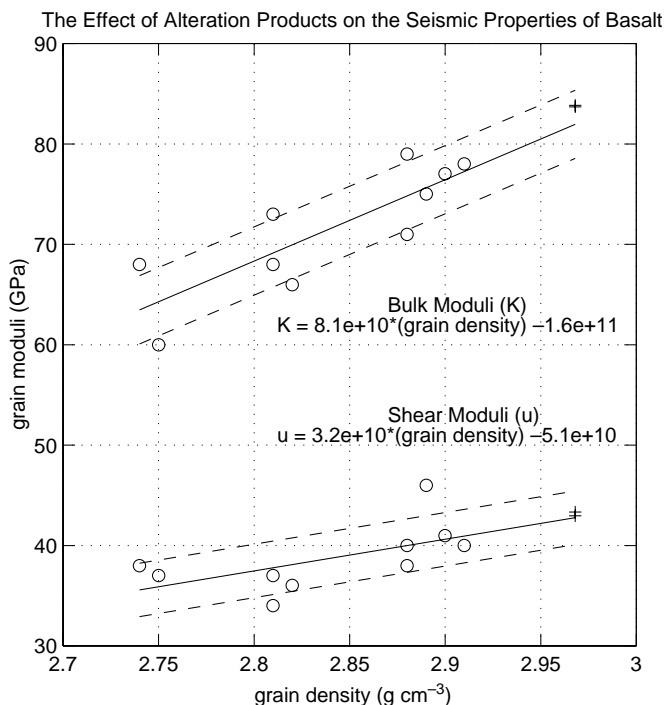


Figure 6. Bulk and shear grain moduli vs. grain density derived from the inversions of the high-pressure *P*- and *S*-wave data for all of the samples. A decrease in grain density corresponds to an increase in alteration products. The correlation shown between grain moduli and grain density suggests that an increase in alteration lowers the grain moduli. A least-squares-fit (solid line) is shown along with one standard deviation bounds (dashed lines). The standard deviations for the fits to the bulk and shear moduli are 3.4 and 2.7 GPa, respectively. Also shown are the Hashin-Shtrikman bounds (crosses) for a zero-porosity rock composed of 50% plagioclase and 50% augite. (The bulk and shear moduli used for plagioclase are 75 and 34 GPa, and those used for augite are 96 and 58 GPa [Christensen, 1982]). The Hashin-Shtrikman bounds fall within one standard deviation of the least-squares-fit line, suggesting consistency between these modeling results and the theory of Hashin and Shtrikman (1963).

m<sup>-3</sup> (a 7.7% reduction), the *P*-wave velocity lowers from 6.85 to 6.36 km s<sup>-1</sup> (a 7.1% reduction), and the *S*-wave velocity lowers from 3.85 to 3.66 km s<sup>-1</sup> (a 5.0% reduction).

## CONCLUSIONS

The effect of cracks and mineralogy on the seismic velocities of subaerially erupted basalts from the Southeast Greenland margin were modeled using the pore aspect ratio theory of Kuster and Toksöz (1974). The influence that cracks, or voids, have on the seismic velocities was separated from the effects of the apparent grain moduli. The principal results of this research can be summarized as follows:

1. Crack modeling of the seismic velocities of slightly altered samples from the interiors of lava flows from Hole 990A showed similar aspect ratio spectra among the samples. Forward calculations using an average, normalized aspect ratio spectrum (Table 3) fit the seismic velocity data for each sample to within an RMS misfit of < 0.050 km s<sup>-1</sup> (< 2%).
2. The percentage of total porosity with aspect ratios ≤ 0.01 (thin cracks) is lower in the more altered samples than in the less altered ones, even though the bulk porosity is higher in the more

altered samples. This suggests that low aspect ratio pores (cracks) are the first portion of the pore space to be filled by alteration products.

- The addition of low grain density alteration products (e.g., clays) into a basalt lowers the grain density and apparent grain bulk and shear moduli of the rock and, thus, lowers its  $P$ - and  $S$ -wave velocities.

## ACKNOWLEDGMENTS

The authors are grateful to N.I. Christensen and his laboratory staff for making the excellent high-pressure velocity and density measurements used in this study. We are also grateful to the reviewers, Matthew Salisbury, Tim Minshull, and Hans-Christian Larsen. Their helpful suggestions significantly improved the paper. This research was funded by the Joint Oceanographic Institutions, United States Science Advisory Committee (JOI/USSAC).

## REFERENCES

- Adams, L.H., and Williamson, E.D., 1923. The compressibility of minerals and rocks at high pressure. *J. Franklin Inst.*, 195:475–529.
- Barton, C., Moos, D., and Blangy, J.-P., 1989. Analysis of full waveform acoustic logging data at ODP Site 642—outer Vøring Plateau. In Eldholm, O., Thiede, J., Taylor, E., et al., *Proc. ODP, Sci. Results*, 104: College Station, TX (Ocean Drilling Program), 953–964.
- Berge, P.A., Fryer, G.J., and Wilkens, R.H., 1992. Velocity-porosity relationships in the upper oceanic crust: theoretical considerations. *J. Geophys. Res.*, 97:15239–15254.
- Berryman, J.G., 1980. Long-wavelength propagation in composite elastic media. *J. Acoust. Soc. Am.*, 68:1809–1831.
- Berryman, J.G., and Berge, P.A., 1996. Critique of two explicit schemes for estimating elastic properties of multiphase composites. *Mech. Mater.*, 22:149–164.
- Birch, F., 1960. The velocity of compressional waves in rocks to 10 kilobars, 1. *J. Geophys. Res.*, 65:1083–1102.
- Birch, F., 1961. The velocity of compressional waves in rocks to 10 kilobars, 2. *J. Geophys. Res.*, 66:2199–2224.
- Carlson, R.L., and Gangi, A.F., 1985. Effect of cracks on the pressure dependence of  $P$ -wave velocities in crystalline rocks. *J. Geophys. Res.*, 90:8675–8684.
- Carlson, R.L., and Herrick, C.N., 1990. Densities and porosities in the oceanic crust and their variations with depth and age. *J. Geophys. Res.*, 95:9153–9170.
- Cheng, C.H., and Toksöz, M.N., 1979. Inversion of seismic velocities for the pore aspect ratio spectrum of a rock. *J. Geophys. Res.*, 84:7533–7543.
- Christensen, N.I., 1982. Seismic velocities. In Carmichael, R.S. (Ed.), *Handbook of Physical Properties of Rocks* (Vol. 2): Boca Raton, FL (CRC Press), 1–228.
- Christensen, N.I., Blair, S.C., Wilkens, R.H., and Salisbury, M.H., 1980. Compressional wave velocities, densities, and porosities of basalts from Holes 417A, 417D, and 418A, Deep Sea Drilling Project Legs 51–53. In Donnelly, T., Francheteau, J., Bryan, W., Robinson, P., Flower, M., Salisbury, M., et al., *Init. Repts. DSDP*, 51, 52, 53 (Pt. 2): Washington (U.S. Govt. Printing Office), 1467–1471.
- Christensen, N.I., and Salisbury, M.H., 1985. Seismic velocities, densities and porosities of Layer 2B and Layer 2C basalts from Hole 504B. In Anderson, R.N., Honnorez, J., Becker, K., et al., *Init. Repts. DSDP*, 83: Washington (U.S. Govt. Printing Office), 367–370.
- Christensen, N.I., Wepfer, W.W., and Baud, R.D., 1989. Seismic properties of sheeted dikes from Hole 504B, ODP Leg 111. In Becker, K., Sakai, H., et al., *Proc. ODP, Sci. Results*, 111: College Station, TX (Ocean Drilling Program), 171–176.
- Duncan, R.A., Larsen, H.C., Allen, J.F., et al., 1996. *Proc. ODP, Init. Repts.*, 163: College Station, TX (Ocean Drilling Program).
- Dvorkin, J., and Nur, A., 1996. Elasticity of high-porosity sandstones: theory for two North Sea data sets. *Geophysics*, 61:1363–1370.
- Eshelby, J.D., 1957. The determination of the elastic field of an ellipsoidal inclusion, and related problems. *Proc. R. Soc. London A*, 241:376–396.
- Gangi, A.F., 1978. Variation of whole and fractured rock permeability with confining pressure. *Int. J. Rock Mech. Min. Sci.*, 15:249–257.
- , 1981. The variation of mechanical and transport properties of cracked rock with pressure. *Proc. U.S. Symp. Rock Mech.*, 22:88–89.
- Hashin, Z., and Shtrikman, S., 1963. A variational approach to the theory of the elastic behaviour of multiphase materials. *J. Mech. Phys. Solids*, 11:127–140.
- Iturrino, G.J., 1995. A study of the nature of oceanic crustal reflectivity using laboratory and log measurements: based on results from Deep Sea Drilling Project and Ocean Drilling Program sites in the Pacific and Indian Oceans [Ph.D. thesis]. Univ. of Miami, Rosenstiel Sch. of Mar. and Atmos. Sci.
- Ju, J.W., and Chen, T.M., 1994. Micromechanics and effective moduli of elastic composites containing randomly dispersed ellipsoidal inhomogeneities. *Acta Mechan.*, 103:103–121.
- Kuster, G.T., and Toksöz, M.N., 1974. Velocity and attenuation of seismic waves in two-phase media, Part I: theoretical formulations. *Geophysics*, 39:587–606.
- Mal, A.K., and Knopoff, L., 1967. Elastic wave velocities in two-component systems. *J. Inst. Math. Applic.*, 3:376–387.
- Mori, T., and Tanaka, K., 1973. Average stress in matrix and average elastic energy of materials with misfitting inclusions. *Acta Metal.*, 21:571–574.
- Planke, S., 1994. Geophysical response of flood basalts from analysis of wireline logs: Ocean Drilling Program Site 642, Vøring volcanic margin. *J. Geophys. Res.*, 99:9279–9296.
- Planke, S., and Cambray, H., 1998. Seismic properties of flood basalts from Hole 917A downhole data, southeast Greenland volcanic margin. In Saunders, A.D., Larson, H.C., Clift, P.D., and Wise, S.W., Jr. (Eds.), *Proc. ODP, Sci. Results*, 152: College Station, TX (Ocean Drilling Program), 453–462.
- Shipboard Scientific Party, 1987. Site 642: In Eldholm, O., Thiede, J., Taylor, E., et al., *Proc. ODP, Init. Repts.*, 104: College Station, TX (Ocean Drilling Program), 53–453.
- , 1994. Site 917: In Larsen, H.C., Sanders, A.D., Clift, P.D., et al., *Proc. ODP, Init. Repts.*, 152: College Station, TX (Ocean Drilling Program), 107–158.
- , 1996. Site 990: In Duncan, R.A., Larsen, H.C., Allen, J.F., et al., *Proc. ODP, Init. Repts.*, 163: College Station, TX (Ocean Drilling Program), 47–68.
- Toksöz, M.N., Cheng, C.H., and Timur, A., 1976. Velocities of seismic waves in porous rocks. *Geophysics*, 41:621–645.
- Tosaya, C.A., 1982. Acoustical properties of clay-bearing rocks [Ph.D. thesis]. Stanford Univ.
- Wilkens, R.H., Christensen, N.I., and Slater, L., 1983. High-pressure seismic studies of Leg 69 and 70 basalts. In Cann, J.R., Langseth, M.G., Honnorez, J., Von Herzen, R.P., White, S.M., et al., *Init. Repts. DSDP*, 69: Washington (U.S. Govt. Printing Office), 683–686.
- Wilkens, R.H., Fryer, G.J., and Karsten, J., 1991. Evolution of porosity and seismic structure of upper oceanic crust: importance of aspect ratios. *J. Geophys. Res.*, 96:17891–17995.

**Date of initial receipt: 8 January 1998**

**Date of acceptance: 18 June 1998**

**Ms 163SR-106**